Structure of a trimeric nucleoporin complex reveals alternate oligomerization states

Vivien Nagy, Kuo-Chiang Hsia, Erik W. Debler, Martin Kampmann, Andrew M. Davenport, Günter Blobel[1], and André Hoelz[1]

Laboratory of Cell Biology, Howard Hughes Medical Institute, The Rockefeller University, 1230 York Avenue, New York, NY 10065

Contributed by Günter Blobel, August 19, 2009 (sent for review July 6, 2009)

The heptameric Nup84 complex constitutes an evolutionarily conserved building block of the nuclear pore complex. Here, we present the crystal structure of the heterotrimeric Sec13·Nup145C·Nup84 complex, the centerpiece of the heptamer, at 3.2-Å resolution. Nup84 forms a U-shaped α-helical solenoid domain, topologically similar to two other members of the heptamer, Nup145C and Nup85. The interaction between Nup84 and Nup145C is mediated via a hydrophobic interface located in the kink regions of the two solenoids that is reinforced by additional interactions of two long Nup84 loops. The Nup84 binding site partially overlaps with the homo-dimerization interface of Nup145C, suggesting competing binding events. Fitting of the elongated Z-shaped heterotrimer into electron microscopy (EM) envelopes of the heptamer indicates that structural changes occur at the Nup145C·Nup84 interface. Docking the crystal structures of all heptamer components into the EM envelope constitutes a major advance toward the completion of the structural characterization of the Nup84 complex.

electron microscopy docking | nuclear pore complex | protein-protein interaction | X-ray crystallography | binding promiscuity

The nuclear pore complex (NPC) represents one of the largest proteinaceous assemblies in eukaryotic cells (≈60 MDa in yeast, ≈120 MDa in vertebrates) and mediates a multitude of diverse transport events between the nucleus and the cytoplasm (1, 2). While small molecules are capable of freely diffusing through the NPC, large particles, such as soluble proteins exceeding approximately 40 kDa, mRNAs, preribosomal particles, and viruses, require a signal-mediated active transport machinery (3–7). A related transport mechanism is responsible for the import of inner nuclear membrane proteins, which are synthesized into the endoplasmic reticulum and outer nuclear membrane (8). In addition to its central role in nucleocytoplasmic transport, the NPC is involved in various other important functions, such as chromatin organization, regulation of transcription, and DNA repair (9–12).

The NPC is composed of approximately 30 different nucleoporins (nups), which are organized into several subcomplexes (13–15). In cells with open mitosis, the NPC is disassembled either into individual nups or various subcomplexes (16–18). A prominent example for such a subcomplex is the extensively studied yeast Nup84 complex. Initially, a hexameric Nup84 complex consisting of Nup84, Nup120, Nup85, Sec13, Seh1, and Nup145C was isolated by biochemical dissection of strains containing tagged proteins (19). Subsequently, Nup133 was identified as a seventh member of the complex isolated under modified conditions (20–22).

Two-dimensional negative-stain electron microscopy (EM) on the heptamer assembled from recombinant proteins revealed an approximately 400-Å-long Y-shaped complex and established the relative position of its members (21) (Fig. 1*A*). The seven nups are arranged in a linear fashion with Nup133 and Nup84 at the base, the Sec13·Nup145C pair in the center, followed by Nup120 and the Seh1·Nup85 pair at the upper arms of the Y. Optimization of the purification protocol yielded a pure heptamer that allowed negative-stain three-dimensional EM (23). This analysis identified specific hinge regions at which the heptamer shows great flexibility, and allowed for the docking of atomic structures of its components into the EM envelope: the Nup133 N-terminal domain (24), Nup107·Nup133 (Nup107 is the human homolog of Nup84) (25), Sec13·Nup145C (26), and Seh1·Nup85 (27).

Although the conformation of the heptamer as well as its higher-order organization in the symmetric NPC core is unknown at present, the heptamers have been suggested to serve as "membrane curving modules," similar to the members of the COPI, COPII, and clathrin coats (28). Interestingly, Sec13 is shared between the NPC and the COPII cage, where it forms the outer coat layer in complex with Sec31 (29–33). Remarkably, the heptamer shares architectural principles with the clathrin triskelion (23), and the molecular model of the COPII cage includes an elongated, curved Sec13·Sec31 hetero-octamer that possesses similar architectural features to the Sec13·Nup145C and Seh1·Nup85 hetero-octamers, which indicates a common evolutionary origin and suggests a physiological relevance of the hetero-octameric assemblies (26–29, 33).

We hypothesized that the elongated, curved Sec13·Nup145C and Seh1·Nup85 hetero-octamers form vertical rods in a fence-like coat for the nuclear pore membrane (26, 27). Most recently, structural and functional analyses of Nup120 identified an interaction with Nup133 and confirmed its physiological relevance. These findings indicate a head-to-tail arrangement of elongated Nup84 complexes into a ring structure and, thus, provide a first glimpse of potential higher-order structures of the heptamer in the NPC (34).

To further advance our knowledge of the molecular architecture and assembly of the heptameric Nup84 complex, we determined the crystal structure of the Sec13·Nup145C·Nup84 heterotrimer, the centerpiece of the heptamer. Extending previous work in which only nucleoporin pairs were depicted, this structure captures the association of three nucleoporins. We find that the U-shaped solenoids of Nup84 and Nup145C bind to each other via their kink regions to form an elongated Z-shaped assembly. Surprisingly, the Nup84 binding site of Nup145C partially overlaps with the region that is also involved in Sec13·Nup145C homo-dimerization. We demonstrate biochemically that Nup84, like Nup145C, exists in a dynamic equilibrium between monomers and dimers in solution. Thus, binding promiscuity may not only occur in Nup145C, but also in other nucleoporins, and offers a molecular basis for structural rear-

Author contributions: V.N. and A.H. designed research; V.N., K.-C.H., E.W.D., A.M.D., and A.H. performed research; V.N., K.-C.H., E.W.D., M.K., G.B., and A.H. analyzed data; and V.N., E.W.D., G.B., and A.H. wrote the paper.

The authors declare no conflict of interest.

Data deposition: The atomic coordinates and structure factors have been deposited in the Protein Data Bank, www.pdb.org (PDB ID code 3IKO).

[1]To whom correspondence may be addressed. E-mail: blobel@rockefeller.edu or hoelza@rockefeller.edu.

This article contains supporting information online at www.pnas.org/cgi/content/full/0909373106/DCSupplemental.

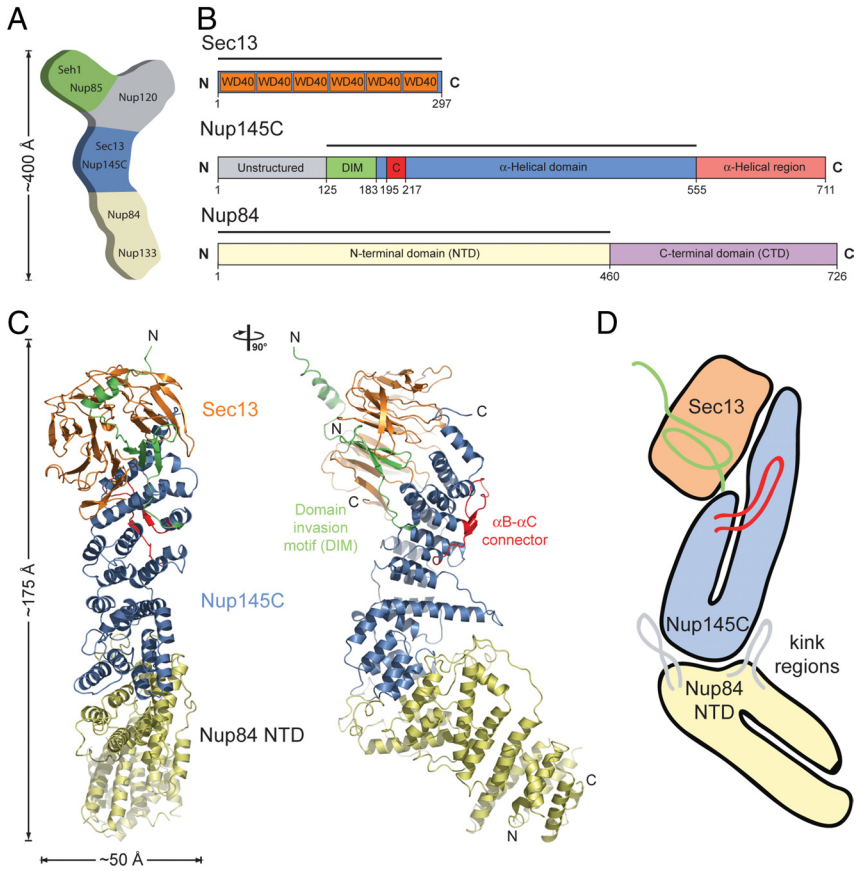

Fig. 1. Structure of the *S. cerevisiae* Sec13·Nup145C·Nup84 NTD complex. (*A*) Schematic representation of the heptameric complex and the approximate localization of its seven nups (21). (*B*) Domain structures of Sec13, Nup145C, and Nup84. For Sec13, the six WD40 repeats (orange) are indicated. For Nup145C, the unstructured N-terminal region (gray), the domain invasion motif (DIM) (green), the αB-αC connector (C) (red), the α-helical domain (blue), and the C-terminal α-helical region (pink) are indicated. For Nup84, the N-terminal domain (NTD) and C-terminal domain (CTD) are indicated. The residue numbering is shown below and the bars above the domain structures mark the crystallized fragments of the three proteins. (*C*) Structure of Sec13·Nup145C·Nup84 NTD in ribbon representation, colored as in panel *B*. A 90°-rotated view is shown on the right. (*D*) Schematic representation of the Sec13·Nup145C·Nup84 NTD heterotrimer.

rangements that are necessary for the NPC to perform its manifold functions.

Results

Structure Determination. To investigate the domain organization of *Saccharomyces cerevisiae* Nup84, we performed sequence conservation analysis and secondary structure predictions. Nup84 is comprised of 726 residues and predicted to be an all-α-helical protein that can be divided into two domains, separated by an ≈30-residue linker. Accordingly, we designed a series of expression constructs for the N-terminal domain (NTD)—the major part of Nup84—and identified a stable fragment composed of residues 1–460 (Fig. 1*B*). We refer to this fragment as the Nup84 NTD in the remainder of the text. The Nup84 NTD tightly interacts with the Sec13·Nup145C nucleoporin pair, and heterotrimer formation is independent of the unstructured N-terminal 124 residues, as well as the C-terminal 156-residue α-helical region of Nup145C. Crystals of the ≈140-kDa *S. cerevisiae* Sec13·Nup145C·Nup84 NTD heterotrimer, containing full-length Sec13, the Nup145C N-terminal domain invasion motif (DIM) and α-helical domain (residues 125–555), and the Nup84 NTD, appeared in the orthorhombic space group $P2_12_12_1$ (Fig. 1*B*). The structure was solved by multiple isomorphous replacement anomalous scattering (MIRAS), using X-ray diffraction data from two heavy-metal derivatives. The asymmetric unit of the crystals harbored three copies of the Sec13·Nup145C·Nup84 NTD heterotrimer (Fig. S1). The structure was refined to 3.2-Å resolution to an R_{cryst} and an R_{free} of 23.4% and 27.3%, respectively. For details of the data collection and refinement statistics, see Table S1.

Analysis of the Oligomeric State. The Sec13·Nup145C nucleoporin pair exists in dynamic equilibrium between heterotetramers and hetero-octamers in solution (26). Moreover, heterotetramer and hetero-octamer formations are predominantly the result of Nup145C and Sec13 homo-dimerization, respectively (26). To determine the oligomerization states of the Nup84 NTD and the Sec13·Nup145C·Nup84 NTD complex in solution, we used analytical size-exclusion chromatography, analytical ultracentrifugation, and multiangle light scattering. Both the Nup84 NTD and the Sec13·Nup145C·Nup84 NTD complex elute from a gel filtration column as two peaks with apparent molecular weights of 80/190 kDa and 215/560 kDa, respectively (Fig. S2 *A* and *B*). The elution positions at molecular weights higher than calculated are likely due to the elongated shapes of the particles. In fact, size-exclusion chromatography coupled with multiangle light scattering revealed that the major Nup84 NTD peak corresponds to a monomer (≈50 kDa) that exists in equilibrium with a minor population of a dimeric state (≈100 kDa) (Fig. S2*C*). Similar results have been obtained for the Sec13·Nup145C·Nup84 NTD complex that exists in equilibrium between the heterotrimer (≈126 kDa) and small amounts of its dimer (≈249 kDa) (Fig. S2*D*). Consistent with these results, analytical ultracentrifugation corroborated the Nup84 NTD

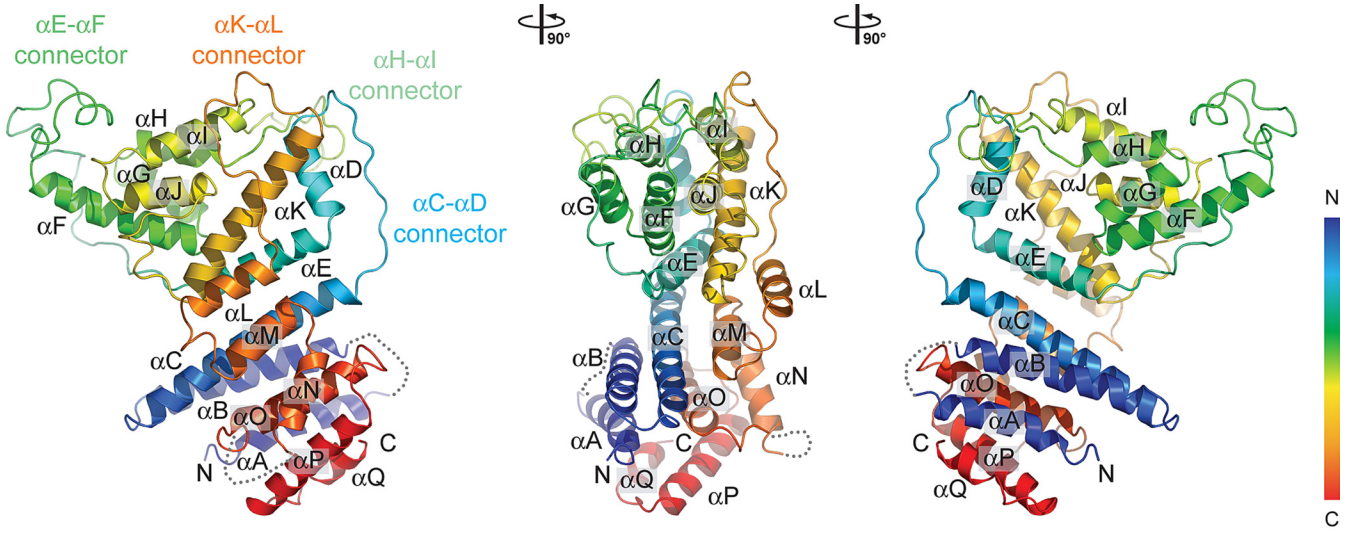

Fig. 2. The Nup84 α-helical domain. Ribbon representation of the Nup84 NTD is shown in rainbow colors along the polypeptide chain from the N- to the C-terminus. The four loops that participate in the Nup145C·Nup84 interaction are indicated.

monomer and the Sec13·Nup145C·Nup84 NTD heterotrimer as the primary species in solution with molecular weights of ≈57 kDa and ≈134 kDa, respectively (Fig. S2*E*). Due to the small fraction of the dimeric species in solution combined with the low protein concentration dictated by analytical ultracentrifugation, the dimeric species were only barely detectable by this technique. The results of the experiments on the oligomeric states are summarized in Table S2.

Architectural Overview. The heterotrimeric Sec13·Nup145C·Nup84 NTD complex forms an elongated, Z-shaped assembly of approximately 175 Å length and approximately 50 Å width with the α-helical solenoid domain of Nup145C at its center (Fig. 1 *C* and *D* and Movies S1 and S2). At one end of the complex, Nup145C invades the Sec13 β propeller with its N-terminal DIM, complementing the six propeller blades of Sec13 with an additional, seventh blade. Notably, the architecture of the yeast Sec13·Nup145C heterodimer is essentially identical to that of the chimeric complex formed between human Sec13 and yeast Nup145C (26). At the other end of the complex, the Nup84 NTD is attached to Nup145C and protrudes at an angle of ≈40° with respect to the long axis of the Sec13·Nup145C complex. The Nup84 NTD adopts an α-helical solenoid fold that is organized in a U-shaped manner (Fig. 1*D*). In the Sec13·Nup145C·Nup84 NTD complex, the two solenoid domains of Nup84 and Nup145C interact with each other in a head-to-head orientation via their kink regions.

The Nup84 α-Helical Domain. The compact U-shaped α-helical solenoid domain of the Nup84 NTD (Fig. 2) resembles the topology of the α-helical solenoid domains of Nup145C and Nup85, two other nucleoporins of the heptameric complex (26, 27). The majority of the Nup84 NTD α helices are arranged in an antiparallel manner, with helices αA-E forming the descending arm of the U, while helices αL-Q represent the ascending arm. In further analogy to Nup85 and Nup145C, the intervening helices αF-K in the kink region of the U form a distinct unit that is connected with the remaining part of Nup84 NTD via two long loops, αE-αF and αK-αL, respectively (Fig. 2). The Nup84 NTD features another two extended connectors, αC-αD and αH-αI, respectively. All four connectors are involved in a finger-like binding to Nup145C to various degrees.

The Nup84 NTD surface has a striking negative surface potential, similar to other members of the heptamer (24–27) (Fig. 3). Two of the few conserved hydrophobic patches fall into the area that contacts Nup145C, and are located toward the periphery of the extended interface (Fig. 3 and Fig. S3). The

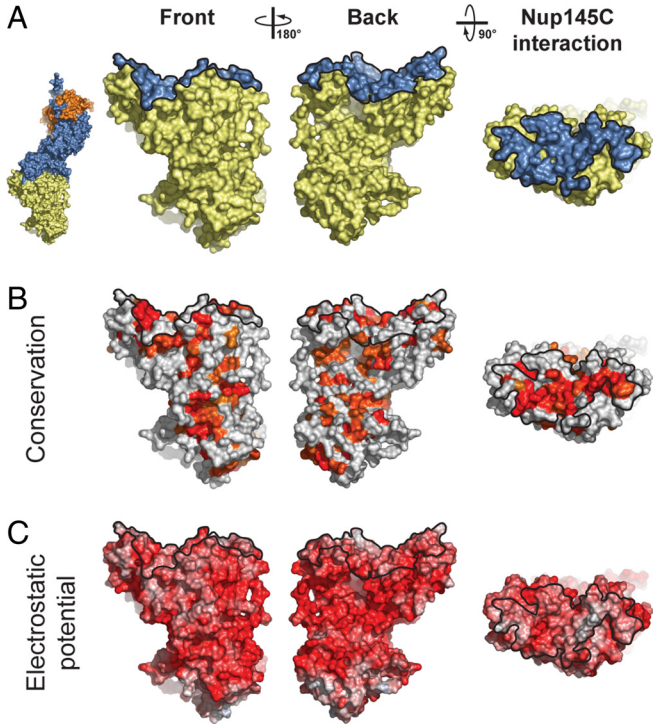

Fig. 3. Surface properties of the Nup84 NTD. The surface orientations are identical in all columns. A black line encircles the Nup145C interaction surface. (*A*) Surface rendition of the Nup84 NTD. The Nup145C contact surface is colored in blue, while the remaining surface is colored in yellow. As a reference, a surface rendition of the heterotrimer is shown to the left, colored according to Fig. 1*C*. (*B*) Surface representation colored according to a multispecies sequence alignment, ranging from 60% similarity (white) to 100% identity (red) (Fig. S4). (*C*) Surface rendition colored according to the electrostatic potential, ranging from −10 k_BT/e (red) to + 10 k_BT/e (blue). Note the two conserved hydrophobic patches located toward the periphery of the extended Nup145C-interacting surface.

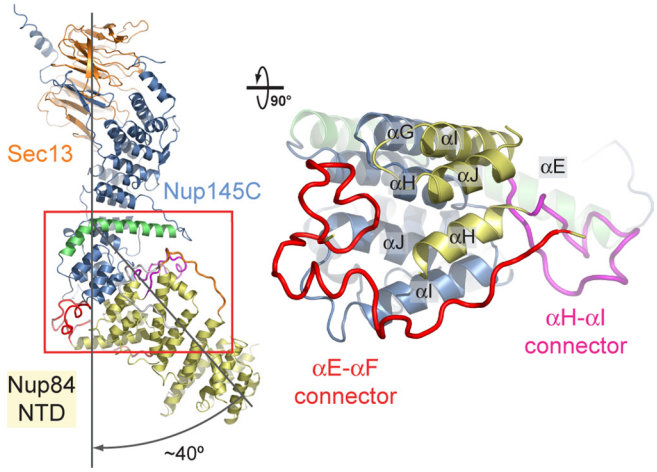

Fig. 4. Interaction of the Nup84 NTD with the Nup145C solenoid domain. The Sec13·Nup145C·Nup84 NTD heterotrimer is shown in ribbon representation, colored according to Fig. 1*C*. The kink regions of the two solenoids interact in a head-to-head fashion. The Nup84 NTD protrudes with an approximate 40° angle from the Nup145C U-shaped solenoid. The inset marks the Nup145C·Nup84 interface that is illustrated in detail on the right. For clarity, the interface shown on the right is rotated by 90°. For Nup145C, the solenoid subdomain (blue) and helix αE (green) are indicated. For Nup84, the interface helices (yellow), as well as the long αE-αF (red) and αH-αI (magenta) connectors that mediate the interaction with Nup145C are indicated.

Nup145C binding area of Nup84 NTD is the largest contiguous conserved region on Nup84 NTD, consistent with its role in Nup145C binding (Fig. 3). Various smaller conserved patches are distributed over the entire Nup84 NTD surface.

The Nup145C·Nup84 Interface. The Nup84 NTD and the Sec13·Nup145C nucleoporin pair associate with each other via the kink regions of their U-shaped solenoid domains (Fig. 4). The interaction is primarily mediated by a hydrophobic patch that is formed by helices αH and αI of Nup84. The two helices bind into a surface groove on Nup145C that is generated by helices αG, αH, αI, and αJ, burying approximately 1,400 Å^2 of surface area. This core interface is augmented by four Nup84 loops, with major contributions from the αE-αF and αH-αI and minor contributions from the αC-αD and αK-αL connectors, burying an additional 1,300 Å^2 of surface area. While the αH-αI loop contacts the long bent helix αE of Nup145C, the αE-αF loop folds into a compact coil structure that contacts the side of the Nup145C kink region (Fig. 4). In total, 2,700 Å^2 of surface area are buried between the two proteins. In accordance with the extensive interactions between the Sec13·Nup145C pair and the Nup84 NTD, the dissociation constant as determined by isothermal titration calorimetry amounts to approximately 7 nM (Fig. S4).

Although the four surface loops contribute to the interface, they appear to play a minor role in the association between the two proteins, since the alteration of the electrostatic character of two key Nup84 residues (I206D and M210D), located in helix αH in the central hydrophobic interface, abolishes the interaction with Nup145C (35). Likewise, a variant of Nup145C in which three residues in helix αH are mutated (V320E, S323E, and Y324A) fails to interact with Nup84 (35).

Binding Promiscuity of Nup145C. In absence of Nup84, the Sec13·Nup145C nucleoporin pair can oligomerize into a hetero-octameric bent pole with comparable dimensions to the hetero-octameric Seh1·Nup85 assembly (26, 27) (Fig. 5*A*). Oligomerization of Sec13·Nup145C is facilitated by homo-dimerization of Sec13 and Nup145C. The homo-dimerization of Nup145C is

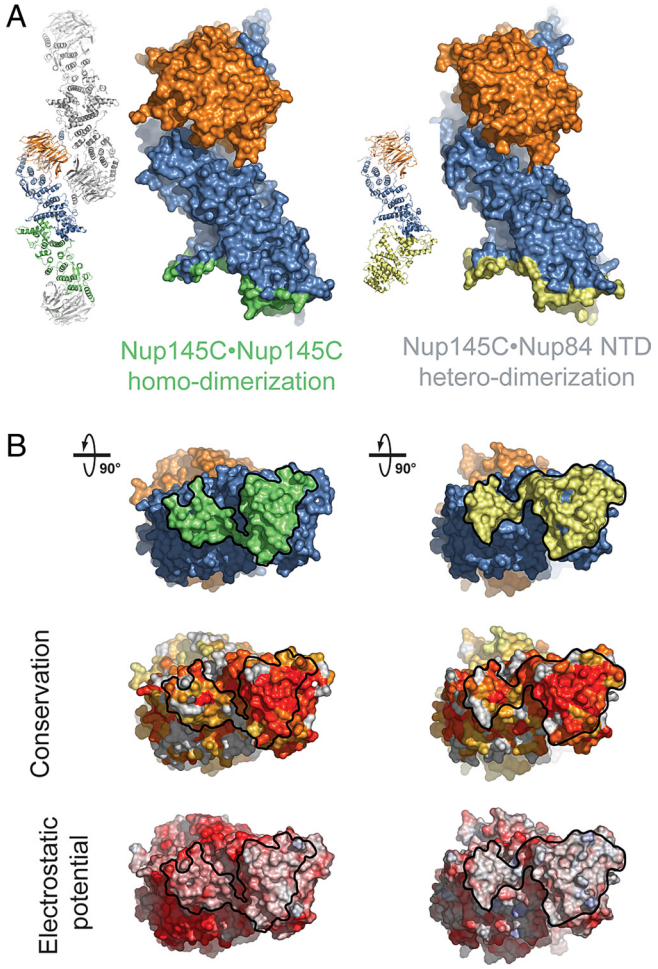

Fig. 5. Binding promiscuity of Nup145C. (*A*) Surface rendition of the Sec13·Nup145C nucleoporin pair derived from the Sec13·Nup145C hetero-octamer (Nup145C·Nup145C homo-dimerization) and the Sec13·Nup145C·Nup84 NTD heterotrimer (Nup145C·Nup84 NTD hetero-dimerization). The Nup145C homo-dimerization and hetero-dimerization surfaces are colored in green and yellow, respectively. The Sec13 and the remaining Nup145C surfaces are colored in orange and blue, respectively. (*B*) 90°-rotated views of the Sec13·Nup145C pair colored according to panel *A* (top), to a multispecies sequence alignment, ranging from 60% similarity (white) to 100% identity (red) (26) (middle), and to the electrostatic potential, from −10 k_BT/e (red) to +10 k_BT/e (blue). The orientation of all surface representations is identical in each column. As a reference, black lines encircle the Nup145C homo-dimerization and Nup84-interaction surfaces.

mediated by a large conserved and hydrophobic surface located in the kink region of the Nup145C solenoid that buries approximately 2,700 Å^2 of surface area (Fig. 5*B*). The Nup145C dimerization interface features a 2-fold rotational symmetry and is generated by the long bent helix αE and the small subdomain at the base of the U-shaped solenoid (helices αF–J). Strikingly, Nup145C utilizes the same structural elements for Nup84 NTD binding so that the Nup84 binding site partially overlaps with the Nup145C homo-dimerization region (Fig. 5*B*). While the Nup145C·Nup145C interaction engages both helix αE and the subdomain, the Nup145C·Nup84 interaction primarily occurs via the subdomain. These findings suggest that Nup145C homo-dimerization and Nup145C·Nup84 hetero-dimerization are competing binding events.

Upon Nup84 binding, conformational changes occur in Nup145C (Fig. S5). While Sec13 and the upper part of the U-shaped Nup145C solenoid form a rigid unit that is not perturbed by the binding of Nup84, the subdomain at the base

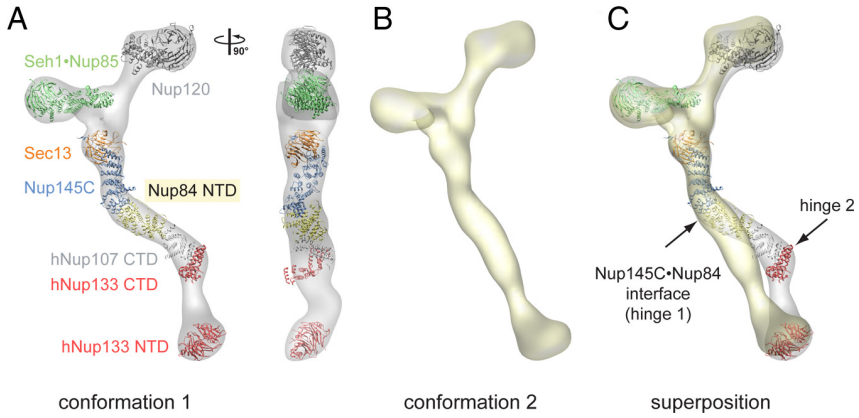

Fig. 6. Protein arrangement within the heptameric complex. (*A*) Docking of crystal structures into the EM envelope of the heptameric Nup84 complex. A 90°-rotated view is shown on the right. The approximate 40° angle by which the Nup84 NTD protrudes from the Sec13·Nup145 nucleoporin pair nicely follows one of the two kink regions of the heptamer stem. (*B*) EM envelope of the second reconstructed conformation of the heptamer in which the two hinge regions are completely extended, forming an almost entirely straight stem. (*C*) Superposition of the two determined heptamer conformations. The kink region at the Nup145C·Nup84 interface is indicated and was used for the structural alignment, showing that this interface corresponds to a hinge in the heptamer stem.

of the solenoid undergoes a rigid body rotation by approximately 6° around the kink in the bent helix αE. This rotation translates into a lateral shift of the subdomain residues that participate in the interaction with Nup84 by approximately 2 Å. Overall the two Sec13·Nup145C structures superimpose with a root-mean square deviation of approximately 1.5 Å over 646 Cα atoms.

Docking of Crystal Structures Into the EM Envelope of the Heptamer. The overall shape of the Nup84 complex and the approximate location of its seven components was established by two-dimensional negative-stain EM in conjunction with protein-protein interaction studies (21). In a recently established three-dimensional negative-stain EM reconstruction of the heptamer marked flexibility at two hinge regions was revealed and two distinct conformations were determined (23). Moreover, the known crystal structures of its components, the Sec13·Nup145C pair, Seh1·Nup85 pair, the human Nup107 CTD·Nup133 CTD complex (Nup107 is the homolog of Nup84), and the human Nup133 NTD were docked into the EM envelope (23).

Here, we have fitted crystal structures of Sec13·Nup145C·Nup84 NTD, a large Nup120 fragment (34), the Seh1·Nup85 pair (27), the human Nup107 CTD·Nup133 CTD complex (25), and the human Nup133 NTD (34) into the EM envelopes of the two conformations (Fig. 6). Nup120 can be docked into both conformers and fits well into the larger of the two upper arms, with the β propeller domain at the end of the arm, and the α-helical domain directed toward the heptamer center. The position of the β propeller coincides with the donut-shaped density observed in the negative-stain structure (23). While the overall Z-shape of the Sec13·Nup145C·Nup84 NTD heterotrimer confirmed the approximate placement of the Sec13·Nup145C pair into the heptamer, it only fits snugly into one of the two determined conformations of the heptamer (Fig. 6 and Movie S3). The approximate 40° angle by which Nup84 NTD protrudes from Nup145C nicely follows one of the two hinges (hinge 1) in the heptamer stem. The comparison with the second conformation, in which the heptamer stem is almost entirely straight, requires an approximate 40° rotation of Nup84 in the Nup145C·Nup84 interface region (Fig. 6). In one scenario, the Nup145C solenoid subdomain may rotate as a rigid body together with Nup84, leaving the core of their interface intact (Fig. 4). Alternatively, the different conformations may be achieved by substantial structural changes or rearrangements at the Nup145C·Nup84 interface. However, the three independent Sec13·Nup145C·Nup84 complexes in the crystal align with an rmsd of ≈1.5 Å over 1,098 Cα atoms, indicating that the observed heterotrimer conformation is not affected by crystal packing. Hence, the molecular basis of the flexibility awaits further elucidation.

Discussion

In an effort to advance our understanding of the architecture of the NPC, we determined the crystal structure of the Sec13·Nup145C·Nup84 NTD heterotrimer, a centerpiece of the evolutionarily conserved heptameric Nup84 complex. The structure extends previous work in which only two interacting nucleoporins were depicted. The docking of the heterotrimer and crystal structures of the other heptamer components into EM envelopes now provides a nearly complete atomic picture of the Nup84 complex. In combination with biochemical and biophysical analyses of the heterotrimer and its components, these data suggest that substantial structural rearrangements can occur within the heptamer.

The structure of Nup84 NTD revealed an α-helical domain with a U-shaped topology. Nup84 binding to the Sec13·Nup145C nucleoporin pair is achieved by the head-to-head interaction of the two kink regions of the U-shaped solenoids of Nup145C and Nup84. A comparison of the Sec13·Nup145C·Nup84 NTD structure with three-dimensional EM structures of the heptamer shows that structural rearrangements or alterations are likely to occur at the Nup145C·Nup84 interface region to explain the flexibility of the heptamer stalk. However, it is not clear yet whether—and if so which one of—these heptamer conformations exist in vivo and to what extent the presence of other nups affect its conformation in the assembled NPC.

The Nup84-binding site partially overlaps with the Nup145C homo-dimerization region that was identified in the Sec13·Nup145C crystal structure (26). In the absence of Nup84, the dimerization of Nup145C and Sec13 leads to the formation of a hetero-octamer (26). Intriguingly, we find that Nup84 NTD, like Nup145C, exists in a dynamic equilibrium between monomers and dimers in solution. Given that these proteins homo-dimerize despite more than a billion years of evolution, these self-associations are likely to be physiologically relevant. This finding then raises the question, at which stage the various assembly states occur: during synthesis and/or storage in the cytoplasm, during NPC assembly, or in the assembled NPC as functional intermediates. For example, Nup84 binding to the Nup145C homo-dimerization region in a chaperone-like fashion may be required to prevent oligomerization of the heptamer in the cytoplasm, and may be altered by adjacent nucleoporins

during assembly and/or function of the NPC (36). Alternatively, the Nup145C·Nup84 interaction could be required for capping of the coat for the nuclear pore membrane at the peripheral rings (26, 27, 34). Notably, the binding promiscuity of Nup145C is a complicating factor for in vivo analyses, in which the common binding surface is mutated, as it cannot be discerned which of the alternate oligomerization states is responsible for the resulting phenotypes. Promiscuous binding events as described here for Nup145C potentially also exist in other nucleoporins, and have already been demonstrated to occur in Sec13 (26, 29).

Structural changes of the central channel have been proposed and described to occur during nucleocytoplasmic transport (37–39). By contrast, a detailed molecular description of comparable changes in the peripheral part of the NPC core is thus far lacking, although large structural rearrangements must occur during the import of integral membrane proteins to the inner nuclear membrane (8). Since the import of the membrane-embedded cargo is mediated by soluble transport factors that travel through the central channel (8), the core of the NPC must slice open during this process.

Crystallographic analyses of nucleoporin oligomers have so far provided valuable snapshots. The acquisition of more still frames, and of oligomers of even higher order, can be expected to yield a more thorough understanding of the dynamics of assembly and function of this most versatile of transport organelles.

Short Methods. The details of molecular cloning, expression, purification, crystallization, X-ray diffraction data collection, structure determination, protein interaction analysis, isothermal titration calorimetry, multiangle light scattering, analytical ultracentrifugation, and docking of crystal structures into the EM map of the heptamer are described in the *SI Text*. In short, the Nup84 NTD was expressed by using a pET28a vector modified to contain a PreScission protease-cleavable N-terminal hexahistidine tag (40). The Sec13·Nup145C complex was expressed using the bicistronic pETDuet-1 (Novagen) expression vector. Recombinant proteins were purified using several chromatographic techniques. Initial phases were determined using a $[Ta_6Br_{12}]^{2+}$ cluster derivative and SAD measurements (40–42). Combined phasing using isomorphous K_2OsO_4 and SeMet SAD and native datasets was carried out in SHARP (43), followed by density modification in DM (44), with solvent flattening, histogram matching, and NCS averaging. Data collection and refinement statistics are summarized in Table S1.

ACKNOWLEDGMENTS. We thank A. Patke, H.-S. Seo, and T. Strowig for discussions and comments on the manuscript; S. Etherton for help with editing the manuscript; D. King for mass spectrometry analysis; and S. Kuebler (Wyatt Technology) and S. Solmaz for assistance with the multiangle light scattering analysis. Edman sequencing was carried out by J. Fernandez at the Rockefeller University Proteomics Resource Center. Analytical ultracentrifugation and isothermal titration calorimetry were carried out by L. Eisele at the Wadsworth Center Biochemistry Core Facility and by S. Bevers at the Biophysics Core Facility at the University of Colorado Denver, respectively. In addition, we thank M. Becker, R. Sanishvili, and R. Fischetti (APS); J. Dickert, S. Morton, K. Royal, and C. Ralston (ALS); and W. Shi (NSLS), for support during data collection. E.W.D. is the Dale F. and Betty Ann Frey Fellow of the Damon Runyon Cancer Research Foundation (DRG-1977-08). A.H. was supported by a grant from the Leukemia and Lymphoma Society.

1. Reichelt R, et al. (1990) Correlation between structure and mass distribution of the nuclear pore complex and of distinct pore complex components. *J Cell Biol* 110:883–894.
2. Pemberton LF, Paschal BM (2005) Mechanisms of receptor-mediated nuclear import and nuclear export. *Traffic* 6:187–198.
3. Hoelz A, Blobel G (2004) Cell biology: Popping out of the nucleus. *Nature* 432:815–816.
4. Debler EW, Blobel G, Hoelz A (2009) Nuclear transport comes full circle. *Nat Struct Mol Biol* 5:457–459.
5. Cook A, Bono F, Jinek M, Conti E (2007) Structural biology of nucleocytoplasmic transport. *Annu Rev Biochem* 76:647–671.
6. Chook YM, Blobel G (2001) Karyopherins and nuclear import. *Curr Opin Struct Biol* 11:703–715.
7. Stewart M (2007) Ratcheting mRNA out of the nucleus. *Mol Cell* 25:327–330.
8. King MC, Lusk CP, Blobel G (2006) Karyopherin-mediated import of integral inner nuclear membrane proteins. *Nature* 442:1003–1007.
9. Blobel G (1985) Gene gating: A hypothesis. *Proc Natl Acad Sci USA* 82:8527–8529.
10. Jani D, et al. (2009) Sus1, Cdc31, and the SacIII CID region form a conserved interaction platform that promotes nuclear pore association and mRNA export. *Mol Cell* 33:727–737.
11. Capelson M, Hetzer MW (2009) The role of nuclear pores in gene regulation, development and disease. *EMBO Rep* 10:697–705.
12. Nagai S, et al. (2008) Functional targeting of DNA damage to a nuclear pore-associated SUMO-dependent ubiquitin ligase. *Science* 322:597–602.
13. Cronshaw JM, Krutchinsky AN, Zhang W, Chait BT, Matunis MJ (2002) Proteomic analysis of the mammalian nuclear pore complex. *J Cell Biol* 158:915–927.
14. Rout MP, et al. (2000) The yeast nuclear pore complex: Composition, architecture, and transport mechanism. *J Cell Biol* 148:635–651.
15. Suntharalingam M, Wente SR (2003) Peering through the pore: Nuclear pore complex structure, assembly, and function. *Dev Cell* 4:775–789.
16. Belgareh N, et al. (2001) An evolutionarily conserved NPC subcomplex, which redistributes in part to kinetochores in mammalian cells. *J Cell Biol* 154:1147–1160.
17. Loïodice I, et al. (2004) The entire Nup107–160 complex, including three new members, is targeted as one entity to kinetochores in mitosis. *Mol Biol Cell* 15:3333–3344.
18. Vasu S, et al. (2001) Novel vertebrate nucleoporins Nup133 and Nup160 play a role in mRNA export. *J Cell Biol* 155:339–354.
19. Siniossoglou S, et al. (1996) A novel complex of nucleoporins, which includes Sec13p and a Sec13p homolog, is essential for normal nuclear pores. *Cell* 84:265–275.
20. Allen NP, Huang L, Burlingame A, Rexach M (2001) Proteomic analysis of nucleoporin interacting proteins. *J Biol Chem* 276:29268–29274.
21. Lutzmann M, Kunze R, Buerer A, Aebi U, Hurt E (2002) Modular self-assembly of a Y-shaped multiprotein complex from seven nucleoporins. *EMBO J* 21:387–397.
22. Siniossoglou S, et al. (2000) Structure and assembly of the Nup84p complex. *J Cell Biol* 149:41–54.
23. Kampmann M, Blobel G (2009) Three-dimensional structure and flexibility of a membrane-coating module of the nuclear pore complex. *Nat Struct Mol Biol* 16:782–788.
24. Berke IC, Boehmer T, Blobel G, Schwartz TU (2004) Structural and functional analysis of Nup133 domains reveals modular building blocks of the nuclear pore complex. *J Cell Biol* 167:591–597.
25. Boehmer T, Jeudy S, Berke IC, Schwartz TU (2008) Structural and functional studies of Nup107/Nup133 interaction and its implications for the architecture of the nuclear pore complex. *Mol Cell* 30:721–731.
26. Hsia KC, Stavropoulos P, Blobel G, Hoelz A (2007) Architecture of a coat for the nuclear pore membrane. *Cell* 131:1313–1326.
27. Debler EW, et al. (2008) A fence-like coat for the nuclear pore membrane. *Mol Cell* 32:815–826.
28. Devos D, et al. (2004) Components of coated vesicles and nuclear pore complexes share a common molecular architecture. *PLoS Biol* 2:2085–2093.
29. Fath S, Mancias JD, Bi X, Goldberg J (2007) Structure and organization of coat proteins in the COPII cage. *Cell* 129:1325–1336.
30. Lederkremer GZ, et al. (2001) Structure of the Sec23p/24p and Sec13p/31p complexes of COPII. *Proc Natl Acad Sci USA* 98:10704–10709.
31. Stagg SM, et al. (2006) Structure of the Sec13/31 COPII coat cage. *Nature* 439:234–238.
32. Stagg SM, LaPointe P, Balch WE (2007) Structural design of cage and coat scaffolds that direct membrane traffic. *Curr Opin Struct Biol* 17:221–228.
33. Stagg SM, et al. (2008) Structural basis for cargo regulation of COPII coat assembly. *Cell* 134:474–484.
34. Seo HS, et al. (2009) Structural and functional analysis of Nup120 suggests ring formation of the Nup84 complex. *Proc Natl Acad Sci USA* doi:10.1073/pnas.0907453106.
35. Brohawn SG, Leksa NC, Spear ED, Rajashankar KR, Schwartz TU (2008) Structural evidence for common ancestry of the nuclear pore complex and vesicle coats. *Science* 322:1369–1373.
36. Napetschnig J, Blobel G, Hoelz A (2007) Crystal structure of the N-terminal domain of the human protooncogene Nup214/CAN. *Proc Natl Acad Sci USA* 104:1783–1788.
37. Beck M, Lucić V, Förster F, Baumeister W, Medalia O (2007) Snapshots of nuclear pore complexes in action captured by cryo-electron tomography. *Nature* 449:611–615.
38. Melčák I, Hoelz A, Blobel G (2007) Structure of Nup58/45 suggests flexible nuclear pore diameter by intermolecular sliding. *Science* 315:1729–1732.
39. Akey CW (1995) Structural plasticity of the nuclear pore complex. *J Mol Biol* 248:273–293.
40. Hoelz A, Nairn AC, Kuriyan J (2003) Crystal structure of a tetradecameric assembly of the association domain of Ca2+/calmodulin-dependent kinase II. *Mol Cell* 11:1241–1251.
41. Murakami KS, Masuda S, Campbell EA, Muzzin O, Darst SA (2000) Structural basis of transcription initiation: An RNA polymerase holoenzyme-DNA complex. *Science* 296:1285–1290.
42. Stavropoulos P, Blobel G, Hoelz A (2006) Crystal structure and mechanism of human lysine-specific demethylase-1. *Nat Struct Mol Biol* 7:626–632.
43. de La Fortelle E, Bricogne G (1997) Maximum-likelihood heavy-atom parameter refinement in the multiple isomorphous replacement and multiwavelength anomalous diffraction methods. *Methods Enzymol* 276:472–494.
44. CCP4 (1994) The CCP4 suite: Programs for protein crystallography. *Acta Crystallogr D* 50:760–763.